INTERNATIONAL JOURNAL FOR NUMERICAL METHODS IN FLUIDS
Int. J. Numer. Meth. Fluids 2007; **54**:1201–1214
Published online 16 January 2007 in Wiley InterScience (www.interscience.wiley.com). DOI: 10.1002/fld.1426

Fingering patterns on an expanding miscible drop in a rotating Hele-Shaw cell

Chen-Hua Chen[1,2] and Ching-Yao Chen[1,3,*,†]

[1]*Graduate School of Engineering Science and Technology, National Yunlin University of Science and Technology, Yunlin, Taiwan, Republic of China*
[2]*Department of Automation Engineering, Nan Kai Institute of Technology, Nantou, Taiwan, Republic of China*
[3]*Department of Mechanical Engineering, National Yunlin University of Science and Technology, Yunlin, Taiwan, Republic of China*

SUMMARY

We perform a detailed numerical study for the evolution of an expanding miscible drop in a rotating Hele-Shaw cell. Two mathematical formulations applied to model the coating layer expansion during practical spin-coating process, such as thinning of the layer by cell pressing and drop spreading outward due to injection, are investigated. Including miscible interfacial stresses, we focus on the investigation of dynamical and morphological influences of two different stabilizing parameters: the gap width parameter for the pressing cell and the injecting strength. In the case of a pressing cell, the fingering features of the expanding miscible drop, such as the critical radius, are distinct from those ones in the experiments of spin coating due to the different distributions of the inherent radial velocity. On the other hand, the global interfacial evolutions of an expanding drop with an additional injection bear remarkable resemblances to their immiscible counterparts. The better agreement for an injecting model suggests its appropriateness when we simulate the emerging fingering instabilities in the spin-coating process. Moreover, we investigate the effects of Coriolis force at higher miscible Bond numbers. Coriolis force affects significantly the onset of fingering instability and the tilting angles of fingers. These stable effects are in line with the results from the previous studies for miscible and immiscible flow fields. Copyright © 2007 John Wiley & Sons, Ltd.

Received 20 June 2006; Revised 16 November 2006; Accepted 24 November 2006

KEY WORDS: spin coating; rotating Hele-Shaw cell; fingering instability; numerical simulation

*Correspondence to: Ching-Yao Chen, Department of Mechanical Engineering, National Yunlin University of Science and Technology, 123 University Road, Section 3, Touliu, Yunlin, Taiwan 640, Republic of China.
†E-mail: chingyao@yuntech.edu.tw

Contract/grant sponsor: National Science Council of the Republic of China; contract/grant number: 93-2212-E-224-006
Contract/grant sponsor: Nan kai Institute of Technology of the Republic of China; contract/grant number: 94-C1201-11

1. INTRODUCTION

Fingering patterns of a rotating drop in a Hele-Shaw configuration have been investigated intensively [1–9] since the seminal work by Schwartz [10]. Based on the Hele-Shaw theory, Alvarez-Lacalle *et al.* [2] investigated the interfacial instabilities of immiscible fluids in a rotating cell both experimentally and numerically, in which Coriolis forces are neglected. Finger pinch-off and droplet emission are detected at the low viscosity contrast and the low surface tension in their experiments. The numerical simulations were strikingly similar to the experimental results. They were confident that their experiments were properly described by the Hele-Shaw equations. On the other hand, in the studies of the miscible flow in a rotating cell, many simulations have been conducted [5–9]. However, without available experimental data for validation, some interesting comparisons between miscible and immiscible flows have been made on the basis of analogy in physical mechanisms of individual parameters and qualitative observations. Many qualitative similarities in the fingering patterns between the numerical results of miscible flows and the experimental findings of immiscible ones at the low surface tension [2] have been found. Recently, Chen *et al.* [9] numerically studied this topic in miscible rotating flows with the miscible effective interfacial tension (or the so-called Korteweg stresses), and reported that the fingering patterns remarkably resemble those ones in the immiscible situation [2]. Besides, they validated that the miscible effective interfacial tensions are both qualitatively and quantitatively equivalent to immiscible surface tensions. Chen and Wang [5] numerically studied the miscible rotating flows with injection and showed that the injecting strength of more viscous fluid through the origin reinforces viscous stabilization. Since the additional injection provides a greater increase in radial velocity, this stabilizing force decays as the mixing front is displaced outward. Another Hele-Shaw problem is a time-dependent gap cell, where the upper plate is lifted or pressed uniformly and the plates remain parallel to each other during the process. Chen and Chen [8] studied this miscible rotating cell with a time-dependent gap and reported that the higher pressing rate provides more stable effects by additional squeezing outward flow. However, these studies resulted from a drop without Korteweg stresses.

One of the main motivations to study a rotating drop in the Hele-Shaw cell is due to its potential applications for better understandings of the spinning-coating process. Spin coating is a widely utilized industrial process in which a thin uniform film formation is accomplished by dispensing a liquid drop onto a fast spinning disc. Though the coating flows are characterized by being free surface (3-D) flow and the contact angle effects are important, the approximation by lubrication theory yields a similar physical phenomenon to Hele-Shaw equations when the coating layer is extremely thin. During coating process, the layer of coating fluid keeps thinning and spreads outward, which bears similarities to a rotating drop in a pressing Hele-Shaw cell [8]. In this situation, the drop expands outward rapidly with a decreasing thickness under the action of the centrifugal force. In the meantime, the expanding drop's area also remarkably resembles to a rotating drop with additional injection [5, 6]. These two qualitative similarities of expanding conditions result in an interesting question regarding their appropriateness to simulate the global development of the emerging fingering instabilities in the spin-coating process. Despite the fact that the formation of a capillary ride near the contact line is observed as a precursor to the instability in the experimental works [11–14] about fingering instabilities, Spaid and Homsy [15] demonstrated that the mechanism of the instability is insensitive to the details of the contact line condition by performing an energy analysis. The instability of the capillary ridge arises due to local variations in the fluid thickness, whereby thicker regions of fluid advance more rapidly over

DOI: 10.1002/fld

the substrate. Moreover, the experimental studies [11, 12] on spin coating are in good agreement with lubrication theories for the spreading of Newtonian fluids. In this study, we neglect the local effects of the capillary rides and focus on the evolution of the global fingering pattern. We perform a detailed numerical study for the fingering instabilities of an expanding miscible drop by applying both expanding mechanisms, the pressing cell and the cell with additional injection. First, we will investigate how the gap width parameter of a pressing cell couples to relevant control parameters, leading to interesting dynamical and morphological effects. Second, we will study the influences of additional injection on the morphological properties of the miscible flow in a rotating cell. Finally, evaluations of both the results by comparing the global interface evolution and fingering morphologies of these two cases with the experimental ones obtained from related cases [11–14, 16] of spin coating will be discussed.

2. GOVERNING EQUATIONS

We investigate the interfacial instability of a heavier (density ρ_h) and more viscous (viscosity μ_h) drop with initial diameter D_0, surrounded by a miscible fluid with less density and viscosity which are denoted as ρ_l and μ_l, respectively, in a rotating Hele-Shaw cell as shown in Figure 1. For the case of additional injection, a point source flow with volume strength Q_c per unit depth is injected through the centre of the cell. For the situation l with a time-dependent cell gap, the flow takes place in a narrow space between two flat plates, where the upper plate is pressed downward uniformly at a specified rate. The initial plate spacing is represented by b_0 and $b(t)$ denotes the time-dependent plate–plate distance. An exponentially increasing cell gap width [17, 18] $b(t) = b_0 e^{\hat{a}t}$ is assumed in the present study, where $\hat{a}$ is a pressing control parameter with a negative value ($\hat{a} \leqslant 0$). These physical problems are governed by the set of following equations [6, 8, 17–19]:

$$\nabla \cdot \mathbf{u} = -\frac{\dot{b}(t)}{b(t)} \tag{1}$$

$$\nabla(p + Q) = -\frac{12\mu}{b^2}\mathbf{u} + \rho\hat{\omega}^2\mathbf{x} + 2\rho\hat{\omega}\mathbf{e_z} \times \mathbf{u} + \nabla \cdot (\hat{\delta}(\nabla c)(\nabla c)^{\mathrm{T}}) \tag{2}$$

$$\frac{\partial c}{\partial t} + \mathbf{u} \cdot \nabla c = D\nabla^2 c \tag{3}$$

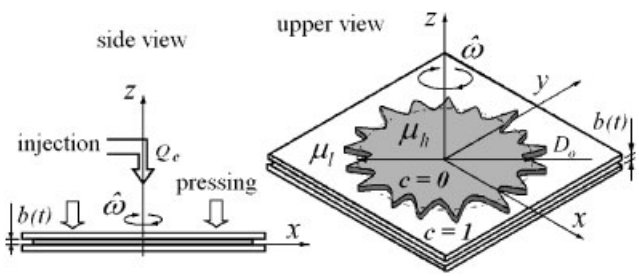

Figure 1. Schematic representation of the miscible fluids in a rotating Hele-Shaw cell with a time-dependent gap.

DOI: 10.1002/fld

Equation (1) expresses a modified incompressible condition that accounts for the pressing of the upper plate [17, 18]. The gap-averaged velocity is expressed by $\mathbf{u}$ and the overdot denotes the total time derivative. A generalized Darcy's law is expressed by Equation (2) where p is the hydrodynamic pressure and Q is the additional pressure due to the Korteweg stresses expressed as [19]

$$Q = \frac{\hat{\delta}}{3}|\nabla c|^2 - \frac{2\delta_2}{3}\nabla^2 c + \frac{2\Delta\rho}{3\rho_h}\mu D\nabla^2 c \tag{4}$$

where δ_2 is the property constant, $\Delta\rho = \rho_h - \rho_l$ denotes the density difference and D the constant diffusion coefficient. The concentration of lighter fluid is represented by c and μ denotes the viscosity, $\hat{\omega}$ the angular speed, $\mathbf{x}$ the position vector on x–y plane, $\mathbf{e_z}$ the unit vector in z-direction and $\hat{\delta}$ the Korteweg stresses coefficient. The superscript $\mathbf{T}$ denotes the transpose. In addition to the conventional viscous term on the right-hand side of this equation, the extra second, third and fourth terms are the centrifugal forces, the Coriolis forces and the miscible effective interfacial tension, respectively. The concentration equation is given by Equation (3). The density and viscosity variations of the mixture are expressed as [7, 18]

$$\rho(c) = c\rho_l + (1-c)\rho_h \tag{5}$$

$$\mu(c) = \mu_l e^{R(1-c)}, \quad R = \ln(\mu_h/\mu_l) \tag{6}$$

where R is the viscosity parameter. In order to render the governing equations dimensionless, we take the diameter D_0 of the drop and the density difference $\Delta\rho = \rho_h - \rho_l$ associated with a dimensionless time of $12\mu_l/b_0^2\Delta\rho\hat{\omega}^2$ as the characteristic scales. By making the governing equations dimensionless, we obtain the dimensionless parameters, such as the Peclet number Pe which can be interpreted as the dimensionless rotating speed, the viscosity Atwood number A representing the viscosity contrast, the Reynolds number Re which includes the effect of the Coriolis forces, the dimensionless Korteweg constant δ that stands for the effects of Korteweg stresses, the gap width pressing parameter a which represents the variety of the dimensionless rate in the gap spacing. The dimensionless parameters take the forms as

$$Pe = \frac{\Delta\rho b_0^2\hat{\omega}^2 D_0^2}{12\mu_l D}, \quad A = \frac{e^R - 1}{e^R + 1}, \quad Re = \frac{\Delta\rho b_0^2\hat{\omega}}{12\mu_l}, \quad \delta = \frac{\hat{\delta}}{\Delta\rho\hat{\omega}^2 D_0^4}, \quad a = \frac{12\hat{a}\mu_l}{\Delta\rho b_0^2\hat{\omega}^2} \tag{7}$$

We split the velocity into a divergence-free component $\mathbf{u_f}$, which is the velocity of the constant spacing and an axisymmetric divergent radial velocity $\mathbf{u_f}$ caused by the gap variation. The divergent radial velocity can be obtained directly as $\mathbf{u_r} = -a\mathbf{r}/2$, which is a potential field. The divergence-free component $\mathbf{u_f} = (u_f, v_f)$ can be acquired by solving the dimensionless governing equations that are obtained in terms of streamfunction ψ and vorticity ω, where streamfunction ψ is further split into the potential component ψ_{pot} and rotational part ψ_{rot}. The dimensionless streamfunction–vorticity formulation and dimensionless equations can be expressed as

$$u_f = \frac{\partial\psi}{\partial y}, \quad v_f = \frac{\partial\psi}{\partial x} \tag{8}$$

$$\nabla^2\psi = -\omega \tag{9}$$

DOI: 10.1002/fld

$$\omega = -R\nabla\psi \cdot \nabla c - \frac{1}{\mathrm{e}^{-2at}\mu}\left(y\frac{\partial c}{\partial x} - x\frac{\partial c}{\partial y}\right) - \frac{2\,Re}{\mathrm{e}^{-2at}\mu}\left(u\frac{\partial c}{\partial x} + v\frac{\partial c}{\partial y} + \rho a\right)$$
$$-\frac{\delta}{\mathrm{e}^{-2at}\mu}\left(\frac{\partial c}{\partial x}\left(\frac{\partial^3 c}{\partial x^2\partial y} + \frac{\partial^3 c}{\partial y^3}\right) - \frac{\partial c}{\partial y}\left(\frac{\partial^3 c}{\partial y^2\partial x} + \frac{\partial^3 c}{\partial x^3}\right)\right) \tag{10}$$

For the situation of additional injection, the analytical distribution of potential radial velocity v_r induced by a point source can be expressed as [5, 6]

$$v_r = \frac{I}{r}, \quad I = \frac{6\mu_1 Q_c}{\pi b_0^2 \Delta\rho\hat{\omega}^2 D_0^2} \tag{11}$$

where I is the dimensionless injecting strength. Boundary conditions are prescribed as follows:

$$x = \pm 2:\ \psi_{\mathrm{rot}} = 0, \quad \frac{\partial c}{\partial x} = 0 \tag{12}$$

$$y = \pm 2:\ \psi_{\mathrm{rot}} = 0, \quad \frac{\partial c}{\partial y} = 0 \tag{13}$$

The initial condition is assumed as a circular shape bounded by a steep concentration gradient in the form of error function. To break the unphysical fingering symmetry, a small magnitude of random perturbations is applied to the positions at $c = 0.5$. In order to obtain extremely fine structures of fingers, a highly accurate pseudospectral method is employed. As a result, the actual boundary conditions applied in the numerical codes at $x = \pm 2$ are modified as $\partial\psi_{\mathrm{rot}}/\partial x = 0$. Under the present situation where no concentration gradient is generated on these boundaries before the calculations terminated, the above conditions automatically lead to $\psi_{\mathrm{rot}} = 0$ and vorticity $\omega = 0$. Both ω and ψ are expanded in a cosine series in the x direction as

$$\psi(x, y, t) = \sum \hat{\psi}_k(y, t)\ \cos[2\pi k x] \tag{14}$$

$$\omega(x, y, t) = \sum \hat{\omega}_k(y, t) \cos[2\pi k x] \tag{15}$$

In the y direction, discretization is accomplished by sixth-order compact finite differences. Vorticity equation is evaluated by sixth-order compact finite difference schemes. The spatial datives in the concentration equation are discretized by sixth- and fourth-order compact finite difference schemes for diffusion terms and convection terms, respectively. A fully explicit third-order Runge–Kutta procedure on time employed to solve concentration equation and advance in time as

$$\frac{\partial c}{\partial t} = F(c) \tag{16}$$

so that

$$c_{i,j}^k = c_{i,j}^{k-1} + \Delta t[\gamma_k F(c_{i,j}^{k-1}) + \eta_k F(c_{i,j}^{k-2})] \tag{17}$$

where $\gamma_1 = \frac{8}{15}$, $\eta_1 = 0$; $\gamma_2 = \frac{5}{12}$, $\eta_2 = -\frac{17}{60}$; $\gamma_3 = \frac{3}{4}$, $\eta_3 = -\frac{5}{12}$. The numerical code is largely identical to the one used in earlier investigations [6, 8, 18, 20, 21], which had been validated by comparing growth rates of small perturbations with linear stability results. More details on the implementation and quantitative validation of these schemes are provided in References [6, 8, 18, 20, 21].

DOI: 10.1002/fld

3. RESULTS AND DISCUSSIONS

In order to link the miscible studies with the immiscible ones that are affected by a dimensionless Bond number Bo, an effective interfacial tension σ_{EIT} will be evaluated and expressed in a dimensionless form of miscible Bond number Bo_{m}. By defining a dimensionless miscible Bond number Bo_{m}, directly qualitative and quantitative comparisons with their immiscible counterparts published in the literatures can be carried out. In addition, agreement between the present results and the findings of immiscible experimental ones could partially validate our numerical simulations. For a typical micro-fabrication practice, the spin coating takes place amid an immiscible interface at a high rotational Bond number. The rotational Bond number (Bo) is defined as

$$Bo = \rho\hat{\omega}^2 V/\sigma \tag{18}$$

where V is the volume of drop and σ is the surface tension. Bo represents a ratio of the centrifugal force to the surface tension. Wang and Chou [14] experimentally studied the fingering instability of a spinning drop at high rotational Bond numbers and reported that the Bond number plays a crucial role in spinning flow. They found that for a high Bo, the number of fingers N_{f} increases rapidly with Bo, while N_{f} is almost independent on Bo for $Bo<50$. In the present situation of miscible interfaces, a miscible Bond number Bo_{m} can be defined by replacing the conventional immiscible surface tension σ in Equation (18) with a miscible effective interfacial tension [9, 22], such as

$$Bo_{\mathrm{m}} = \frac{\pi}{160\sigma_{\mathrm{EIT}}} \tag{19}$$

where

$$\sigma_{\mathrm{EIT}} = \int_M |\delta| \left(\frac{\mathrm{d}c}{\mathrm{d}n}\right)^2 \mathrm{d}n \tag{20}$$

σ_{EIT} is the dimensionless miscible effective interfacial tension [23]. In Equation (20), the integration is taken across (and perpendicularly) the mixing interface (n represents the normal direction to the interface), with M denoting the mixing region. Note that the integrand in Equation (20) is reminiscent of the Korteweg stress contribution appearing as the fourth term at the right-hand side of the generalized Darcy's Law (see Equation (2)). So, the miscible effective interfacial tension is naturally defined by integrating such squared normal gradient of the concentration across the interface. Besides, we assume that the drop approximates a spreading flat disc of fluid and the initial plate spacing $b_0 = R_0/20$ in Equation (19), where R_0 is the initial radius of the drop.

Now, we begin our numerical investigation by performing a series of studies on the concentration images and contours obtained from different values of the control parameters. In order to compare the simulated findings of miscible spinning drops with the immiscible experimental ones, we keep a higher Peclet number $Pe = 2 \times 10^4$, which means weaker diffusive effects or a faster rotating speed, and a higher Atwood number $A = 0.905$ in this study. The A-value indicates that the drop is about 20 times more viscous than the environment. We focus on the effects of both the gap width parameter a and the injecting strength I with various strengths of Korteweg stresses at $\delta = -5 \times 10^{-6}$ and -8×10^{-5} to obtain conditions of both the higher and lower Bo_{m}. Furthermore,

DOI: 10.1002/fld

a typical density ratio at $\rho_h/\rho_l = 100$ is applied to the cases with a non-zero gap width parameter to simplify the problem.

3.1. Simulations of a pressing cell

First, we simulate the case of a pressing cell and introduce stronger Korteweg stresses into the flow, but without additional injected liquid, i.e. $\delta = -8 \times 10^{-5}$ and $I = 0$ for $Pe = 2 \times 10^4$, $A = 0.905$. Figure 2 depicts the interface evolutions for concentration contours of $c = 0.7$ for different pressing rates $a = 0, -0.01, -0.014$ and -0.016 at various time. Figure 2(a) shows a representative calculation of a drop in constant gap spacing cell. After a latency period, the interface develops small ripples, which indicates the initiation of instability. Very vigorous interfacial instability is triggered by the strong centrifugal force after $t \geqslant 25$, which gives rise to a characteristic fingering

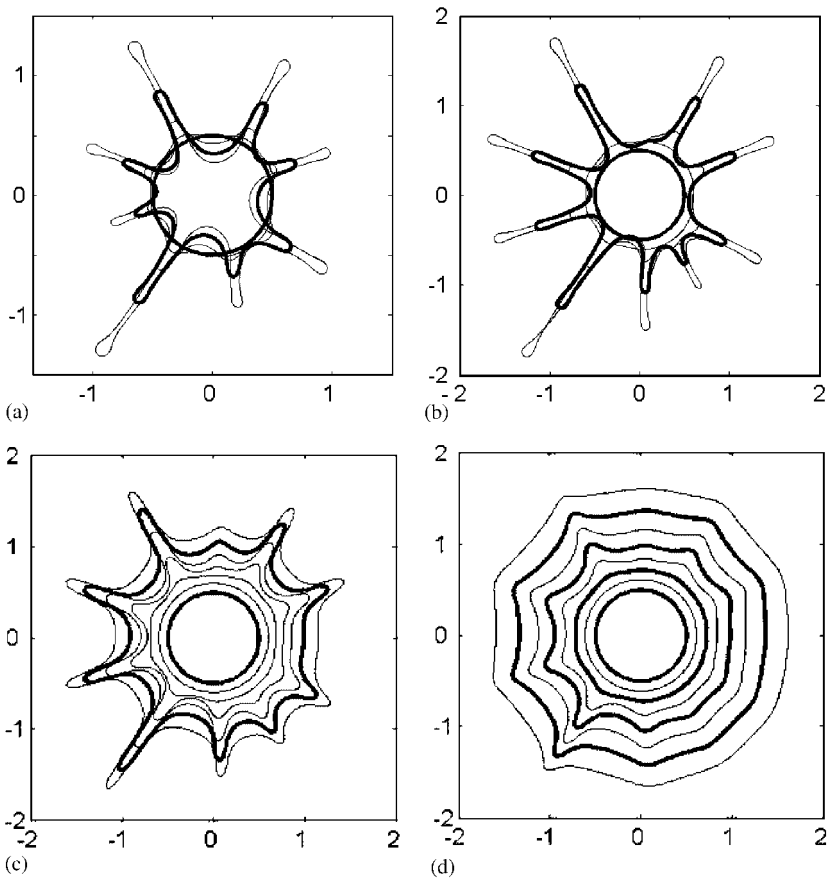

Figure 2. $Pe = 2 \times 10^4$, $A = 0.905$, $\delta = -8 \times 10^{-5}$, and $I = 0$. Interface evolution for concentration contours of $c = 0.7$ in different pressing rate: (a) for $a = 0$, curves at time of 0, 25, 30, 35 and 40 are represented; (b) for $a = -0.01$, curves at time of 0, 30, 45, 60 and 75; (c) for $a = -0.014$, curves at time of 0, 20, 40, 60, 80, 100 and 120; and (d) for $a = -0.016$, curves at time of 0, 20, 40, 60, 80, 100,120 and 140. As the upper plate is pressed at a certain rate, the outward flow of a more viscous fluid provides stable force.

DOI: 10.1002/fld

pattern. Significant inward penetrations on the inner front are also clearly observed. The fingering patterns of this case do resemble the ones obtained by immiscible situation with strong surface tension [1, 4]. In this situation with strong interfacial tensions of $\delta = -8 \times 10^{-5}$, the miscible Bond number is calculated at about $Bo_{\mathrm{m}} = 17$, which is close to the lower values of Bond numbers in the immiscible experiments [11–13]. In the following simulations, we will apply the present value of Korteweg constant to further compare with the experimental findings [11–13].

In Figure 2(b), we set the gap pressing parameter $a = -0.01$. It is known that the displacement of a less viscous fluid (the surrounding fluid in the present situation) by a more viscous fluid (the expanding drop) leads to a stable interface. So, the outward flow of a more viscous fluid provides a stable force as the upper plate is pressed at a certain rate. The interface evolution shows that the interfacial fingering is delayed until $t \geqslant 45$. After the onset of instability, the fingers of outer fluid quickly penetrate inward and finally reach near the circular contacting front of the original drop. On the contrary, for the case of a higher pressing rate $a = -0.016$ as shown in Figure 2(d), the interfacial fingerings are suppressed significantly and the miscible interface is much more stable. If the pressing rate is further raised to $a = -0.02$, it results in a fully stable circular pattern. In these cases, the interfacial morphologies in the outer region are dominated by the competition of three different mechanisms, which are stable viscosity contrast, stable pressing outward velocity and the unstable centrifugal force. On the other hand, the reverse penetration on the inner front is governed by the balance between viscous instability and squeezing outward stability. If we modulate the pressing rate properly, i.e. $a = -0.014$ shown in Figure 2(c), the fingering patterns are significantly similar to those ones in the immiscible experimental results of Melo *et al.* [11] where Bond number is about $Bo = 10$. Also, the interfacial evolution for the concentration contours of $c = 0.7$ is very similar to those ones in the immiscible experimental findings (Figure 4 in Fraysse and Homsy [12]) and numerical results of Schwartz and Roy [24] for Newtonian fluid, where the Bond numbers are about $Bo = 8$. However, in this case the dimensionless critical radius $R_{\mathrm{c}}/R_0 = 1.35$, where R_{c} is the critical radius of the drop at the onset of instability, is much smaller than $R_{\mathrm{c}}/R_0 = 2.0$ which is the immiscible experimental results of Fraysse and Homsy [12]. Besides, the number of fingers remains almost unchanged, i.e. $N_{\mathrm{f}} = 9$, in both Figures 2(b) and (c). This phenomenon that the number of fingers do not increase with the increasing critical radius at a higher pressing rate is inconsistent with the findings in the immiscible experiments [12, 14, 24]. These variations are attributed to the different distributions of the radial velocity. According to the lubrication approximation, the drop radius increases as $t^{1/4}$ in asymptotic regime [11, 12]. Moreover, a power law fit for the experimental data of Fraysse and Homsy [12] suggests a similar approximation of $t^{0.29}$, and the results of Melo *et al.* [11] are approximately as $t^{1/3}$. Hence, the experimental asymptotic radial velocity in spinning drop is inversely proportional to the square of distance away from the origin, i.e. $v_r \sim r^{-2}$ [12]. Nevertheless, at the present pressing cell, the radial velocity is proportional to the radial distance ($v_r \sim r$). The inherent radial velocity distributions appear a fundamental difference. For a sufficient large pressing rate at a later stage, the interface is primarily controlled by the increasing radial pressing velocity. On the other hand, the radial expansion in a typical practical spin-coating process decays as time proceeds. As a result, the interface is predominated by the centrifugal force at a later stage. This discrepancy suggests that a pure pressing cell model is not fully appropriate to simulate the spin-coating processes even though the morphological evolutions show great qualitative similarities in certain cases. For the same reason, when we perform the simulations of a miscible drop with weaker Korteweg stresses (higher Bond numbers) in a pressing cell, the fingering patterns are inconsistent with the immiscible experimental findings of Wang and Chou [14] for higher Bond number.

DOI: 10.1002/fld

3.2. *Effects of injection*

We now focus on the situation with additional injection from the origin. Figure 3 displays the interfacial evolution for the concentration contours of $c = 0.7$ in four different injection strengths with strong Korteweg stresses. Compared with the reference case in Figure 2(a), Figure 3 clearly shows the more stable effects by the injecting flow. The onset time of instability is delayed, and the original circular mixing front is better preserved while expanding outward. Likewise, for smaller injection strength $I = 0.006$ in Figure 3(a), significant inward penetration occurs after the onset of instability, and the fingers rapidly grow outward and finally stretch to the computational boundaries. In addition, it is observed that a stronger injecting strength leads to a larger critical radius R_c and

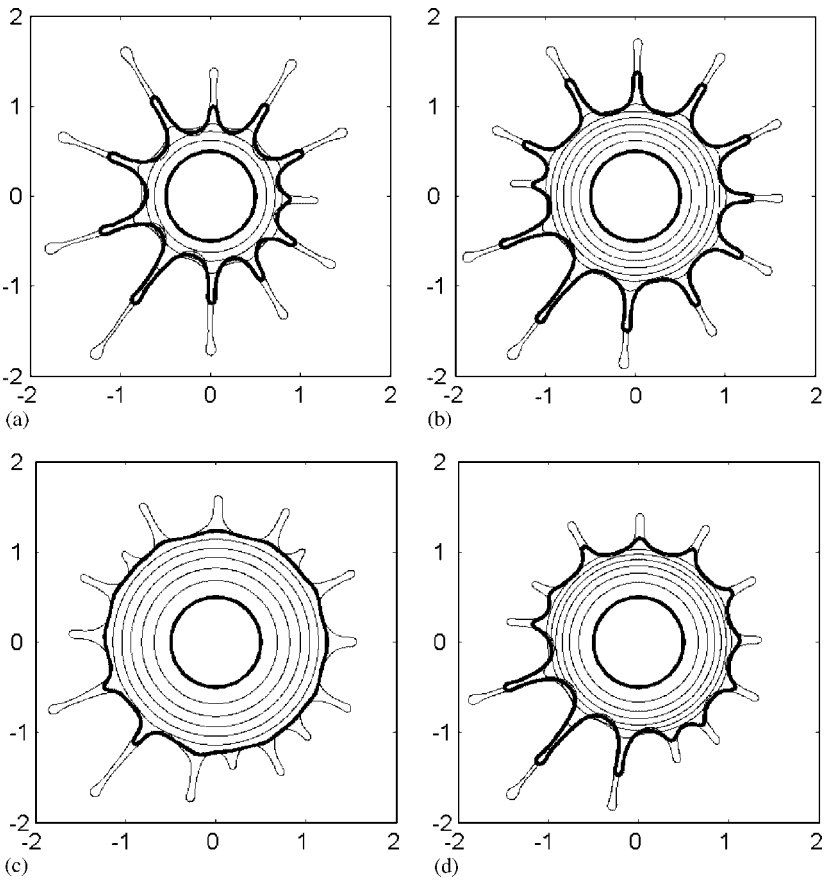

Figure 3. $Pe = 2 \times 10^4$, $A = 0.905$, $\delta = -8 \times 10^{-5}$, $a = 0$, interface evolution for concentration contours of $c = 0.7$ in different injection strength: (a) for $I = 0.006$, curves at time of 0, 10, 20, 30, 35 and 40 are represented; (b) for $I = 0.012$, curves at time of 0, 5, 10, 15, 20, 25, 30, 35 and 38; (c) for $I = 0.02$, curves at time of 0, 5, 10, 15, 20, 25, 30 and 35. More number of fingers and larger critical radius R_c at the stronger injecting strength show that the injecting flow reinforces viscous stabilization; and (d) for $I^* = 0.005$, curves at time of 0, 5, 10, 15, 20, 25, 30, 35 and 38. This interface evolution is very similar to that ones in Figure 3(b).

DOI: 10.1002/fld

more fingers in Figures 3(b) and (c). In line with the common spin-coating phenomena [12, 14, 24], the number of fingers increases as the critical radius increases. With increasing the perimeter of the expanding drop and decreasing the interface curvature and surface tension, more fingers are easily generated. When we modulate the injection strength to $I = 0.012$ as shown in Figure 3(b), the fingering patterns also resemble remarkably the experimental results of Fraysse and Homsy [12] for Newtonian fluid and Spaid and Homsy [13] for a viscoelastic drop. Moreover, the dimensionless critical radius $R_c/R_0 = 1.95$ also approaches the immiscible experimental results of $R_c/R_0 = 2$ by Fraysse and Homsy [12]. In addition, the denser concentration accumulation is found at the fingertip area in Figure 3. Compared with the pressing case in Figure 2(c), Figure 3 shows that the fingertips are rounder in these cases while the fingers become increasingly sharper in Figure 2(c). The pattern of fingertips in Figure 3 is also similar to the ones in the immiscible cases [11, 24]. This phenomenon is attributed to the farther fingers with slow spreading velocity when the flux of injection to the centre of drop is constant. As stated above, the experimental asymptotic radial velocity in spinning drop is inversely proportional to the square of distance away from the origin ($v_r \sim r^{-2}$). In the current case, the magnitudes of inherent radial velocity caused by injection are inversely proportional to the distance away from the origin, c.f. $v_r \sim r^{-1}$, which is more consistent to the experimental measurements. This explains better quantitative agreement for the present injecting model in simulating a spin-coating process.

Since the experimental asymptotic spreading velocity is $v_r \sim r^{-2}$, we carry a simulation by applying this radial velocity profile by modifying the radial velocity distribution shown in Equation (11) as

$$v_r^* = \frac{I^*}{r^2} \tag{21}$$

where I^* is the modified dimensionless injecting strength. All the physical parameters are kept the same as the ones used in Figure 3(b) except replacing I with I^* ($I^* = 0.005$). Figure 3(d) displays the interface evolution of the simulation for the concentration contours of $c = 0.7$. This interface evolution is very similar to those ones in Figure 3(b). Therefore, the above simulations have confirmed that the morphological properties of an expanding drop in a rotating cell with an additional injection lead to better agreement with their immiscible counterparts in spin coating.

3.3. Effects of Korteweg stresses and Coriolis forces

In this section, we turn to investigate the effects of injection in weaker Korteweg stresses cases. Figure 4(a) shows a calculation of a drop with weaker Korteweg stresses, but without additional injected liquid in constant gap spacing cell, i.e. $\delta = -5 \times 10^{-6}$, $I = 0$ and $a = 0$, for $Pe = 2 \times 10^4$, $A = 0.905$. Compared with the similar case with stronger Korteweg stress displayed in Figure 2(a), the weaker miscible effective interfacial tension induces more vigorous interfacial instability. A more irregular reverse penetration on the inner front is observed. According to the estimate by Equation (19), a miscible Bond number is about $Bo_m = 207$. This case of higher miscible Bond number is applied to the simulate results of the miscible spinning drops with the weaker Korteweg stresses in order to compare with the findings [14, 16] of spin coating at a higher rotational Bond number. In Figure 4(b), we apply the injecting strength $I = 0.05$ in the cell. It shows clearly that there are a lot more fingers than the previous simulations. Similar to the case with strong Korteweg stresses, a stronger injecting strength leads to a larger critical radius and more fingers. Figure 5 shows the dimensionless critical radius R_c/R_0 and the number of fingers N_f as a function of the

DOI: 10.1002/fld

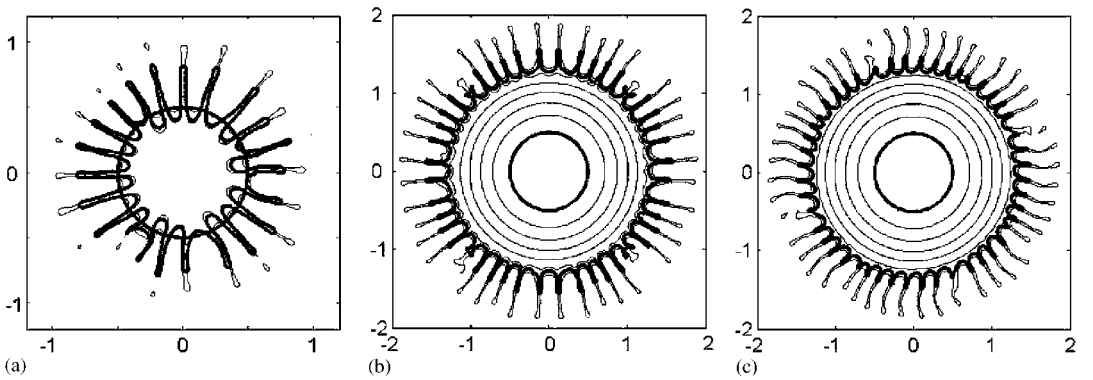

Figure 4. $Pe = 2 \times 10^4$, $A = 0.905$, $\delta = -5 \times 10^{-6}$, $a = 0$, interface evolution for concentration contours of $c = 0.7$: (a) for $I = 0$, $Re = 0$, curves at time of 0, 10, 15 and 17.5 are represented; (b) for $I = 0.05$, $Re = 0$, curves at time of 0, 2.5, 5, 7.5, 10, 12.5, 15 and 17.1; and (c) for $I = 0.05$, $Re = 0.7$, curves at time of 0, 2.5, 5, 7.5, 10, 12.5, 15 and 17.5. It is clearly observed that extremely slim fingers turn counter-clockwise due to the effects of the strong Coriolis force.

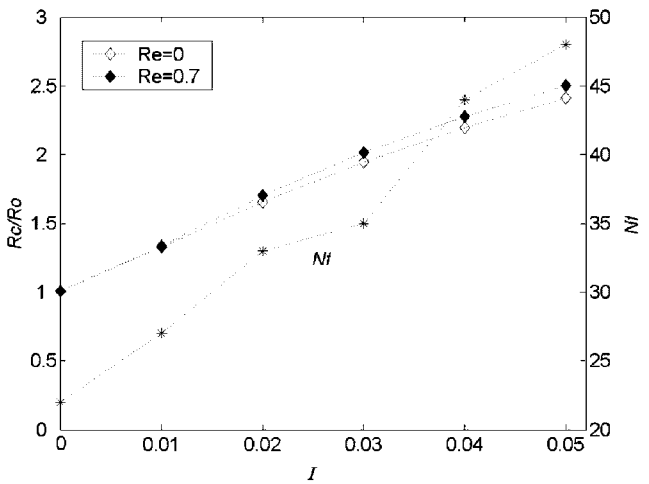

Figure 5. The dimensionless critical radius R_c/R_0 and the number of fingers N_f, as a function of the injecting strength I. It shows that the number of fingers is almost proportional to the perimeter of the expanding drop at the moment of onset. Besides, the fact that Coriolis force can increase the critical radius for the stronger injecting strength is observed.

injecting strength I. The number of fingers is almost proportional to the perimeter of the expanding drop at the moment of onset. Thus, the number of fingers will be larger if a drop can expand to a large radius before the fingering instability starts. These features agree with the practice of spin coating in high Bond number [14]. Besides, like the interfacial evolution of experiments [14] for a typical spin-coating flow with forming fingers at high Bond number, it is observed that the outward flow preferentially runs into these fingers and completely bypasses some portions of the

DOI: 10.1002/fld

substrate. Therefore, we point out that, if Korteweg stresses are taken into account in a rotating miscible case, the interfacial evolutions and morphologies of an expanding drop with an additional injection in a rotating Hele-Shaw cell are strikingly similar to the ones in common spin-coating process.

The Coriolis force plays an important role in spinning flow at high rotational Bond number [14, 16]. Thus, we perform the simulations of a miscible drop with weaker Korteweg stresses to investigate the effects of Coriolis force, in terms of dimensionless parameter Reynolds number Re. It is noteworthy to point that Waters and Cummings' recent studies [25] introduced Coriolis force in a more rigorous fashion onto a 3-D Navier–Stokes equation, and the findings were compared with the ones of the gap-averaged 2-D Darcy's model of Schwartz [10] at the linear level. They reported that inclusion of the Coriolis force into Darcy's law can lead to significant errors at large Reynolds number, while Schwartz predicts approximately at smaller Re. In order to account for the effect of Coriolis force, we keep the Reynolds number fixed at $Re = 0.7$ to match the experimental value of Re in Reference [16] for spinning flow at high rotational Bond number in this study. Figure 4(c) shows the interface evolution for concentration contours of $c = 0.7$ for $Pe = 2 \times 10^4$, $A = 0.905$, $\delta = -5 \times 10^{-6}$, $I = 0.05$ and $Re = 0.7$. Compared with the case in Figure 4(b) without Coriolis force, this pattern shows that the extremely slim fingers turn counter-clockwise due to the effects of the strong Coriolis force. It is important to note that the morphologies observed in this result are remarkably similar to those ones obtained experimentally [16] and numerically for immiscible flow [24]. Cho *et al.* [16] experimentally studied the effects of Coriolis force on fingering instability during spin coating, and reported that Coriolis force affects significantly the onset of fingering instability, the tilting angle and the shape of fingers, and the maximum attainable radius. Consistent findings are obtained and shown in Figure 5, such that for a stronger injecting strength, Coriolis force can delay the critical time and increase the critical radius. These stable effects are in line with the previous studies for miscible [6, 8] and immiscible flow fields [16, 24].

4. CONCLUSION

We have presented the numerical simulations of fingering instabilities on an expanding miscible drop in a rotating Hele-Shaw cell. The investigation intends to evaluate the appropriateness of two mathematical descriptions that are applied to model the coating layer expansion during practical spin-coating process, i.e. thickness thinning by cell pressing and drop spreading outward due to injection. We study the influences of relevant control parameters, focusing on the gap width parameter a, the injecting strength I, the Korteweg stresses δ and Coriolis forces Re. For an expanding drop in a cell of sufficient large pressing rate, the interface is primarily controlled by the radial velocity ($v_r \sim r$), leading to the interfacial instabilities distinct from those ones in the immiscible experiment ($v_r \sim r^{-2}$) due to the significant different distributions of the inherent radial velocity. On the other hand, the fingering features of a rotating drop with an additional injection, such as overall interface evolution and fingering morphologies, bear remarkable resemblances to their immiscible counterparts [11–14] because of a more similar distribution of the inherent radial velocity profile c.f. $v_r \sim r^{-1}$. The results suggest the model with an additional injection is more appropriate to simulate the global development of the emerging fingering instabilities in the spin-coating process. Moreover, we investigate the effects of Coriolis force in the situations of weaker Korteweg stresses (high miscible Bond numbers). For the stronger injecting strength, Coriolis force affects significantly the onset of fingering instability and the tilting angles of fingers. These

DOI: 10.1002/fld

stable effects are in line with the previous studies for miscible [6, 8] and immiscible [16, 24] flow fields.

ACKNOWLEDGEMENTS

C.-Y. Chen thanks the National Science Council of the Republic of China for financial support under grant number 93-2212-E-224-006. C.-H. Chen is supported by Nan Kai Institute of Technology of the Republic of China under grant number 94-C1201-11.

REFERENCES

1. Carrillo L, Magdaleno F, Casademunt J, Ortin J. Experiments in a rotating Hele-Shaw cell. *Physical Review E* 1996; **54**:6260–6267.
2. Alvarez-Lacalle E, Ortin J, Casademunt J. Low viscosity contrast fingering in a rotating Hele-Shaw cell. *Physics of Fluids* 2004; **16**(4):908–924.
3. Gadelha H, Miranda J. Finger competition dynamics in rotating Hele-Shaw cells. *Physical Review E* 2004; **70**:066308.
4. Miranda J, Alvarez-Lacalle E. Viscosity contrast effects on fingering formation in rotating Hele-Shaw flows. *Physical Review E* 2005; **72**:026306.
5. Chen C-Y, Wang S. Interfacial instabilities of miscible fluids in a rotating Hele-Shaw cell. *Fluid Dynamics Research* 2002; **30**(5):315–330.
6. Chen C-Y, Liu Y-C. Numerical simulations of miscible fluids on a rotating Hele-Shaw cell with effects of Coriolis forces. *International Journal for Numerical Methods in Fluids* 2005; **48**(8):853–867.
7. Chen C-Y, Wu H-J. Numerical simulations of interfacial instabilities on a rotating miscible magnetic droplet with effects of Korteweg stresses. *Physics of Fluids* 2005; **17**(4):042101.
8. Chen C-H, Chen C-Y. Numerical simulations of interfacial instabilities on a rotating miscible droplet in a time-dependent gap Hele-Shaw cell with significant Coriolis effects. *International Journal for Numerical Methods in Fluids* 2006; **51**:881–895.
9. Chen C-Y, Chen C-H, Miranda J. Numerical study of pattern formation in miscible rotating Hele-Shaw flows. *Physical Review E* 2006; **73**:046306.
10. Schwartz L. Instabilities and fingering in a rotating Hele-Shaw cell or porous medium. *Physics of Fluids A* 1989; **1**:167–169.
11. Melo F, Joanny JF, Fauve S. Fingering instability of spinning drops. *Physical Review Letters* 1989; **63**(18): 1958–1961.
12. Fraysse N, Homsy GM. A experimental study of rivulet instabilities in centrifugal spin coating of viscous Newtonian and non-Newtonian fluids. *Physics of Fluids* 1994; **6**(4):1491–1504.
13. Spaid MA, Homsy GM. Stability of viscoelastic dynamic contact lines: a experimental study. *Physics of Fluids* 1997; **9**(4):823–832.
14. Wang W, Chou F. Fingering instability and maximum radius at high rotational Bond number. *Journal of the Electrochemical Society* 2001; **148**(5):G283–G290.
15. Spaid MA, Homsy GM. Stability of Newtonian and viscoelastic dynamic contact lines. *Physics of Fluids* 1996; **8**:460–478.
16. Cho H, Chou F, Wang M, Tsai C. Effect of Coriolis force on fingering instability and liquid usage reduction. *Japanese Journal of Applied Physics* 2005; **44**(19):L606–L609.
17. Shelley M, Tian F-R, Wlodarski K. Hele-Shaw flow and pattern formation in a time-dependent gap. *Nonlinearity* 1997; **10**:1471–1495.
18. Chen C-Y, Chen C-H, Miranda J. Numerical study of miscible fingering in a time-dependent gap Hele-Shaw cell. *Physical Review E* 2005; **71**:056304.
19. Hu H, Joseph D. Miscible displacements in a Hele-Shaw cell. *Zeitschrift fur Angewandte Mathematik und Physik* 1992; **43**:626–645.
20. Ruith M, Meiburg E. Miscible rectilinear displacements with gravity override. Part 1: Homogeneous porous medium. *Journal of Fluid Mechanics* 2000; **420**:225–257.
21. Meiburg E, Chen C-Y. High-accuracy implicit finite difference simulations of homogeneous and heterogeneous miscible porous media flows. *SPE Journal* 2000; **5**(2):129–137.

DOI: 10.1002/fld

22. Chen C-Y, Wu H-J, Hsu L. Numerical simulations of labyrinthine instabilities on a miscible elliptical magnetic droplet. *Journal of Magnetism and Magnetic Materials* 2005; **289**:365–367.
23. Chen C-Y, Liu K-T. Numerical simulations of a miscible drop in a spinning drop tensiometer. *Journal of Mechanics* 2007; **23**:1–6.
24. Schwartz L, Roy R. Theoretical and numerical results for spin coating of viscous liquids. *Physics of Fluids* 2004; **16**(3):569–584.
25. Waters SL, Cummings LJ. Coriolis effects in a rotating Hele-Shaw cell. *Physics of Fluids* 2005; **17**:048101.

DOI: 10.1002/fld